Rapid Communications | Editors' Suggestion

# Universal description of III-V/Si epitaxial growth processes

I. Lucci,[1] S. Charbonnier,[2] L. Pedesseau,[1] M. Vallet,[3] L. Cerutti,[4] J.-B. Rodriguez,[4] E. Tournié,[4] R. Bernard,[1] A. Létoublon,[1] N. Bertru,[1] A. Le Corre,[1] S. Rennesson,[5] F. Semond,[5] G. Patriarche,[6] L. Largeau,[6] P. Turban,[2] A. Ponchet,[3] and C. Cornet[1,*]

[1]*Univ Rennes, INSA Rennes, CNRS, Institut FOTON – UMR 6082, F-35000 Rennes, France*

[2]*Univ Rennes, CNRS, IPR (Institut de Physique de Rennes) - UMR 6251, F-35000 Rennes, France*

[3]*CEMES-CNRS, Université de Toulouse, UPS, 29 rue Jeanne Marvig, BP 94347 Toulouse Cedex 04, France*

[4]*IES, Université Montpellier, CNRS, Montpellier, France*

[5]*Université Côte d'Azur, CRHEA-CNRS, Rue Bernard Grégory, F-06560 Valbonne, France*

[6]*Centre de Nanosciences et de Nanotechnologies, Site de Marcoussis, CNRS, Université Paris Sud, Université Paris Saclay, Route de Nozay, F-91460 Marcoussis, France*

(Received 9 April 2018; published 12 June 2018)

Here, we experimentally and theoretically clarify III-V/Si crystal growth processes. Atomically resolved microscopy shows that monodomain three-dimensional islands are observed at the early stages of AlSb, AlN, and GaP epitaxy on Si, independently of misfit. It is also shown that complete III-V/Si wetting cannot be achieved in most III-V/Si systems. Surface/interface contributions to the free-energy variations are found to be prominent over strain relief processes. We finally propose a general and unified description of III-V/Si growth processes, including a description of the formation of antiphase boundaries.

DOI: 10.1103/PhysRevMaterials.2.060401

Integrating monolithically III-V semiconductors on group-IV ones is often considered as the ultimate step for the cointegration of photonics with electronics, such as lasers, passive devices, or multijunction solar cells [1,2]. The main issues of polar on nonpolar epitaxy to overcome were soon identified in the 1980's [3,4]. But since the interplay between three-dimensional (3D) growth modes, strain relaxation, antiphase domains, and other defects was never clarified, researchers preferentially developed defect filtering strategies using thick III-V buffers grown on silicon [5]. Reaching higher photonic integration levels now requires a deep understanding of the processes involved at the early stages of III-V/Si heterogeneous epitaxy.

Summarizing the large literature on the subject is hopeless, but we would like to emphasize three major physical concepts about III-V/Si growth that are usually presented as implicit underlying statements and that are in close relationship with the present work.

First, the origin of antiphase domain (APD) formation is commonly attributed to either Si single steps or an incomplete group-III or group-V initial coverage of the Si surface. This general picture, described in detail by Kroemer [3], is today considered as the main motivation for using misoriented Si substrates, in order to promote bi-step formation, and theoretically hamper the formation of antiphase boundaries.

Second, the origin of the commonly observed 3D islanding during III-V/Si growth was frequently ascribed to strain relaxation processes, for instance, in the case of GaAs on Si [4,6], since most III-V semiconductors are lattice mismatched to the silicon. It was also noticed that for mismatched semiconductors, significant densities of dislocations are generated well before island coalescence. However, 3D islanding was also already reported in quasi-lattice-matched systems such as GaP/Si [7].

Finally, III-V/Si interface atomic arrangement was theoretically addressed on the basis of density functional theory (DFT) calculations. This was, for instance, discussed in relation to GaAs/Si [8] or more recently to GaP/Si [9–11]. Highlights were given on the fact that abrupt III-Si or V-Si interfaces are not always the most stable configurations, depending on the group-III/group-V chemical potentials. Indeed, some charge-compensated interdiffused interfaces following the electron counting model criteria [12] were found to be remarkably stable [9,10,13,14].

In this Rapid Communication, we aim to clarify the main III-V/Si crystal growth processes. From an atomically resolved microscopy analysis, the morphologies of monodomain III-V (AlSb, GaP, or AlN) islands at the Si (001 or 111) surfaces are first established. On the basis of absolute surface/interface energies calculated by *ab initio* (DFT) calculations on GaP/Si, the wetting properties are determined over the full range of the phosphorus chemical potential. The respective contributions of the surface/interface and stress relief to free-energy variation during III-V/Si epitaxy are then compared. We finally describe the main steps of III-V/Si heteroepitaxy and the formation of antiphase domains.

3D islanding is first investigated through three different III-V semiconductor materials because they allow one to span the initial epitaxial stress from compressive (AlSb/Si) to tensile (AlN/Si) through near zero (GaP/Si).

In Fig. 1(a), the scanning transmission electron microscopy (STEM) energy-dispersive x-ray spectroscopy (EDX) images are given for AlSb/Si-6°-off islands (5 nm), buried in a GaSb matrix, with corresponding Ga and Al contrasts. A high-resolution TEM image of the interfacial misfit dislocation

*Corresponding author: charles.cornet@insa-rennes.fr

 

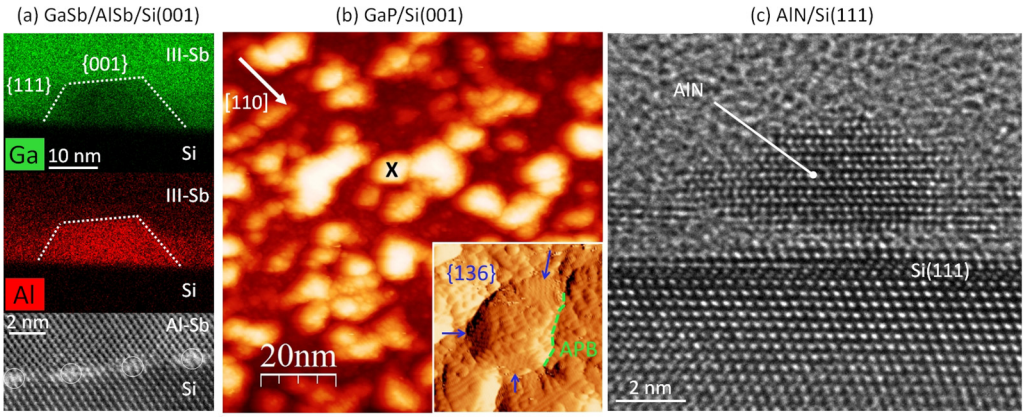


FIG. 1. 3D islanding in various III-V/Si material systems. (a) Cross-sectional STEM-EDX image of GaSb/AlSb layers grown on Si(001)-6°-off, showing the Ga and Al concentrations, and high-resolution STEM imaging of the AlSb/Si interface; dislocations are surrounded. (b) Plan-view STM imaging of a 3-nm-thick GaP deposition on Si(001)-6°-off ($100 \times 100\ \text{nm}^2$; vertical color scale: 0–5.1 nm). The $20 \times 20\ \text{nm}^2$ inset shows the atomically resolved morphology of the individual island marked with a black cross, with {136} facets and an antiphase boundary. STM image was differentiated to enhance atomic contrasts. (c) Cross-sectional high-resolution TEM image of a 2-nm-thick AlN deposition on Si(111).

network is also given. Figure 1(b) displays the scanning tunneling microscopy (STM) in-plane image of a 3-nm GaP/Si-6°-off deposition, a very early stage of growth, as compared to previous studies [15,16]. The inset shows the atomically resolved typical morphology of one individual island at the surface, where {136} facets can unambiguously be identified [17], together with a trench that shows the emergence of an antiphase boundary. Figure 1(c) shows the cross-sectional high-resolution TEM image of 2-nm AlN/Si(111) deposition. Experimental details on growth and microscopy are given in the Supplemental Material [18].

From these experiments, some important conclusions can already be made. First, in the various experiments performed on the three material systems, 3D islands were always observed, and the presence of a wetting layer was not clearly or systematically evidenced [see Figs. 1(a) and 1(c), for instance], which confirms the partial wetting of III-V on Si, i.e., the Volmer-Weber growth mode, independently of the strain state [6,7]. We believe that this is a general behavior of III-V/Si heteroepitaxial systems even when alternated growth techniques are used [18,19]. We will strengthen this assumption later on. Finally, the III-V/Si Volmer-Weber growth mode does not *a priori* hamper the Si surface to be terminated with a single monoatomic layer of group-III, group-V, or another element rising from the epitaxial reactor background. The impact of such a passivating layer will be discussed later.

It is also remarkable that in both AlSb and AlN material systems, the misfit is so large that the III-V material relaxes very rapidly. Even if the relaxation process is not similar in Sb- and N-based materials, complete strain relief is nearly achieved at only 1 nm of the interface. Figure 1(a) also illustrates that the island size is much larger than the typical distances between dislocations. It was already reported that dislocations appear well before the islands coalesce [6], and we note that the observed islands are nearly perfectly faceted well after crystal plastic relaxation. This suggests that the elastic relaxation of strain [20] is not contributing significantly to the energy balance of individual islands. Here, we conclude that surface/interface energies play a crucial role in III-V/Si 3D islanding.

The last important conclusion that can be drawn from the experiments is the monodomain character of the observed single islands. In Fig. 1(b), most of the individual grains have a homogeneous morphology. The largest homogeneous islands (without APDs) are likely a consequence of smaller islands coalescing. Neighboring smaller islands are also visible, with a clear separation between them that seems to hamper the coalescence [shown with the green dashed line in the inset of Fig. 1(b)]. The atomic structure of one individual island shown in the inset of Fig. 1(b) evidences the monodomain character of the island and the presence of {136} facets. Therefore, from cross-sectional TEM and plan-view STM experiments it is clear that individual III-V/Si islands remain monodomains. This observation is in agreement with the work of Akahane *et al.* [21] where individual AlSb or GaSb islands on Si were observed. The anisotropy of individual islands was demonstrated along either the [110] or the $[1\bar{1}0]$ silicon crystallographic axis, demonstrating the monodomain character of the single islands, and the overall bidomain distribution of the island population. The size of the islands presented in Figs. 1(a) and 1(b) is also interesting. Both GaP and AlSb epilayers were grown on Si(001)-6°-off substrates, where atomic (biatomic) steps are separated on average by 1.29 (2.58) nm. Monodomain islands are significantly larger ($\approx$10 nm), which contradicts the usual correlation made between monoatomic Si steps and APB formation [3].

To complete the picture, we note that the average spacing between islands (10 nm) in Fig. 1(b) corresponds well to the APD correlation length measured on the thicker epilayers grown under the same conditions (8–12 nm) [22]. Finally, the impact on the structural quality of III-V/Si epilayers by III-V islands coalescing on them was highlighted [7,23].

In a first and general description, the III-V/Si wetting properties can be examined within the Young-Dupré spreading parameter Ω [24],

$$\Omega = \gamma^{S}_{(\text{Si})} - \gamma^{S}_{(\text{III}-\text{V})} - \gamma^{i}_{(\text{III}-\text{V/Si})}, \quad (1)$$

TABLE I. GaP and Si surface and interface energies computed by DFT.

| Surface/interface | Details | Reconstruction | Energy (meV/Å²) P-rich | Ga-rich |
|---|---|---|---|---|
| Si(001) | Flat | c(2 × 4) | | 92.8 |
| Si(001) | $D_B$ step | p(2 × 2) | | 89.3 |
| Si(001) | $S_B$ step | p(2 × 2) | | 89.2 |
| Si(001) | $S_A$ step | c(2 × 4) | | 87.1 |
| GaP(001) | P-rich | (2 × 4) | 57.4 | 72.4 |
| GaP(001) | Ga-rich | (2 × 4)-md | 82.8 | 52.9 |
| GaP(136) | Type A | (1 × 1) | 52.9 | 62.7 |
| GaP(136) | Type B | (1 × 1) | 66.8 | 57.1 |
| GaP-Si | Abrupt Ga-Si | (1 × 1) | 72.0 | 40.8 |
| GaP-Si | Abrupt P-Si | (1 × 1) | 29.7 | 60.9 |

where $\gamma^S_{(\mathrm{III-V})}$ and $\gamma^S_{(\mathrm{Si})}$ are the surface energies of the most stable III-V facet that would be involved in the two-dimensional (2D) growth on the substrate and of the silicon surface, respectively, and $\gamma^i_{(\mathrm{III-V/Si})}$ is the interface energy between the III-V semiconductor and the Si. A positive value of Ω corresponds to perfect wetting conditions, while a negative value corresponds to partial wetting, i.e., a Volmer-Weber growth, or perfect nonwetting conditions. However, the evaluation of Ω requires the accurate determination of surface and interface energies, which is done for GaP in this work.

To this aim, different absolute surfaces and interface energies of interest were computed via DFT calculations (see the Supplemental Material [18]). The silicon surface energy was already widely discussed [25–27]. Silicon surfaces with or without steps have been considered in this work, and we find that the presence of steps at the silicon surface (at least for a miscut below or equal to 6°) does not significantly change the silicon surface energy range (87–93 meV/Å²). For GaP, the situation is different, as the surface energies depend on the reconstruction of the facet, on the chemical potential, and therefore on the growth conditions used (P or Ga rich). Calculations show that the {136} surface energies of GaP are in the same range as the {001} ones, as already found for GaAs [28]. Finally, abrupt Ga-Si or P-Si (001) GaP/Si interface energies also depend on the chemical potential [9,10]. In a first approximation, we do not consider the charge-compensated interfaces that may further stabilize the interface [10]. The results obtained are summarized in Table I.

The spreading parameter Ω is then plotted in Fig. 2(a) as a function of the phosphorus chemical potential variation $\Delta\mu_P = \mu_P - \mu_P^{\mathrm{P-bulk}}$ ($\mu_P$ is the chemical potential of P atoms, and $\mu_P^{\mathrm{P-bulk}}$ is the chemical potential of P atoms in black phosphorus; see details in Ref. [18]), where the right (left) side corresponds to P-rich (Ga-rich) limit conditions [9].

The calculation is presented both for the P-Si and the Ga-Si abrupt interfaces, with a $D_B$-stepped Si surface. The most stable {001} surface reconstruction was always considered at a given value of the chemical potential, explaining the slope variation of Ω. Regardless of the chemical potential and the interface, Ω remains negative, indicating partial wetting conditions, even if in extreme P-rich conditions with a P-Si abrupt interface, the accuracy of the DFT calculation

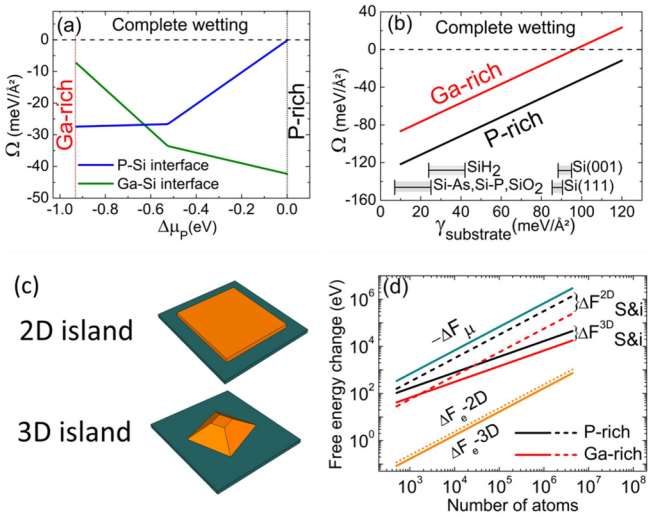


FIG. 2. (a) Spreading parameter vs the chemical potential variation for the deposition of GaP/Si, with P-Si and Ga-Si abrupt interfaces. (b) Spreading parameter vs substrate surface energy in P- and Ga-rich conditions with a Ga-Si interface. (c) Sketch of the 2D (strained) and 3D (elastically relaxed) GaP islands on Si. (d) The different contributions ($\Delta F_\mu$, $\Delta F_{S\&i}$, $\Delta F_e$) to the free-energy variation for 3D and 2D GaP/Si islands with a Ga-Si interface.

does not allow one to conclude unambiguously on the sign of Ω in this very narrow window. Considering that most III-V semiconductors have the same surface energy orders of magnitude, this conclusion (partial wetting conditions) can be extended to most III-V semiconductors deposited on Si. In the following, the abrupt Ga-Si interface will be chosen for illustration.

In Fig. 2(b), the spreading parameter is plotted as a function of the substrate surface energy in P- and Ga-rich conditions. Ω increases with the substrate surface energy, as expected by definition. In the same plot we are also report typical surface energy ranges of some commonly used starting Si surfaces (passivated or unpassivated) already considered in the literature, such as Si(001), Si(111), $SiH_2$, SiAs, SiP, or $SiO_2$ (e.g., Refs. [29] or [30]). Here, Si*X* stands for the *X*-terminated Si surface. The vertical positioning of the different Si*X* surfaces has no physical meaning. The impact of surface pretreatment or orientation on interface energy is not taken into account. We here conclude that any Si surface pretreatment or passivation will tend to stabilize the highly reactive nude Si surface, and thus favor partial wetting conditions, strongly reducing the hope to reach complete III-V/Si wetting conditions in real epitaxial chambers where the passivation can be intentional or nonintentional.

To complete the picture at the submonolayer scale, and evaluate the relative contributions of stress relaxation and surface/interface energies, we now compare two different situations: a strained 2D GaP island (with a one monolayer height, growing laterally) and an elastically relaxed 3D truncated pyramidal GaP island in its Wulf-Kaishew equilibrium shape growing in an homothetic way on the silicon substrate, as depicted in Fig. 2(c). A careful STM image analysis has been performed on the data of Fig. 1(b), which gives an average island height of 2.5 nm, and an average diameter of

11 nm, which leads to an average (miscut included) island contact angle of 27.04°. Among the different stable facets observed with GaP or GaAs materials that are mainly lying around the {001}, {111}, {136}, and {114}ones [17,28], the measured contact angle can only correspond to the {136} ones (theoretical contact angle of 27.8°). We therefore model the GaP 3D islands by truncated pyramidal structures composed of facets with an angle $\alpha = 27.8°$, having the surface energy of {136} facets. As explained in the Supplemental Material [18], the surface energy of this facet is taken from the {2511} one as it is the most stable configuration, and respecting the electron counting model.

The pyramid has a square basis (length $b_1$), a {001} facet on top (length $b_2$), and grows in a homothetic way during the initiation steps. Truncated pyramid islands are chosen at their equilibrium shape determined by the Wulf-Kaishew theorem [31]. From the surface energies determined in Table I, in P-rich conditions, $b_2/b_1 = 0.05$, while in Ga-rich conditions, $b_2/b_1 = 0.60$. For the modeling of the 2D GaP island on Si, we model the top surface by a conventional {001} facet and keep a one monolayer height thickness; the 2D island is only growing laterally. The edge energy is neglected, which gives a lower limit estimated around $10^3$ for the total number of atoms composing the island.

The total free-energy variation during the GaP/Si growth is then calculated for the different 2D or 3D island configurations by using [31]

$$\Delta F_{\mathrm{TOT}} = \Delta F_{\mu} + \Delta F_{e} + \Delta F_{\mathrm{S\&i}}. \tag{2}$$

It corresponds to the difference of free energy between an initial thermodynamic state with a total atom number $N$ related to the sum of Ga and P atoms in a vapor reservoir together with a nude Si substrate, and a final state where the GaP crystal is formed on the Si. The first term is the chemical work needed to form the bulk crystal from an infinite reservoir.

For the molecular beam epitaxy of GaP using a $P_2$ source, it becomes

$$\Delta F_{\mu} = N k_B T \ln\left(\frac{P_{\mathrm{Ga}}\left(P_{\mathrm{P_2}}\right)^{1/2}}{P_{\mathrm{Ga}-\infty}\left(P_{\mathrm{P_2}-\infty}\right)^{1/2}}\right), \tag{3}$$

where $T$ is the growth temperature, $N$ the number of condensed atoms, $P_X$ the partial pressure of species $X$, $P_{X-\infty}$ the saturation partial pressure of species $X$, and $k_B$ the Boltzmann constant. While $T$ and $P_X$ are extracted directly from growth conditions, the saturation pressures have been precisely calibrated in Ref. [32] (Sec. 2.5.4) for GaP. The second term is associated with the elastic energy stored and is defined as

$$\Delta F_{e} = R\mathcal{F}_0 m^2 V = R\Delta F_{e}^{\mathrm{2D}}, \tag{4}$$

where $m$ is the epitaxial misfit between the deposited material and the substrate, $V$ the volume of the deposited crystal, $\mathcal{F}_0$ a combination of the elastic coefficients $C_{ij}$, and $R$ the relaxation energy factor [31]. $\Delta F_e^{\mathrm{2D}}$ is the elastic energy of a biaxially strained 2D layer [31]. Here, we take $R = 1$ for the 2D GaP island growing on Si, and $R = 0.7$ for the free elastic energy variation $\Delta F_e$-3D of the 3D GaP island [33]. Finally, for a cubic crystal stressed in a (001) plane, $\mathcal{F}_0$ is expressed as $(C_{11} + C_{12} - 2\frac{C_{12}^2}{C_{11}})$.

The third term corresponds to the formation of surfaces and interfaces, which is rewritten in the present case,

$$\Delta F_{\mathrm{S\&i}} = \sum_j \gamma^{S}_{(\mathrm{III-V}),j} S_{(\mathrm{III-V}),j} + S_{(\mathrm{III-V/Si})}\left(\gamma^{i}_{(\mathrm{III-V/Si})} - \gamma^{S}_{(\mathrm{Si})}\right), \tag{5}$$

where $\gamma^{S}_{(\mathrm{III-V}),j}$ and $\gamma^{S}_{(\mathrm{Si})}$ are the surface energies of the $j$th III-V facet and of the silicon surface, respectively, $\gamma^{i}_{(\mathrm{III-V/Si})}$ is the interface energy between the III-V semiconductor and the Si, $S_{(\mathrm{III-V}),j}$ the surface of the $j$th III-V facet, and $S_{(\mathrm{III-V/Si})}$ the contact surface between the III-V and the Si. In this work, we neglect the vibrational contribution to the free energy, which is not expected to impact the main conclusions [34].

The $-\Delta F_{\mu}$, $\Delta F_e$, and $\Delta F_{\mathrm{S\&i}}$ are plotted in Fig. 2(d) for both Ga- and P-rich conditions, and for the two types of islands, as a function of an increasing number of atoms. The energy gain provided by the crystal formation $\Delta F_{\mu}$ is partly counterbalanced by both $\Delta F_e$ and $\Delta F_{\mathrm{S\&i}}$, the elastic and surface/interface contributions. A first conclusion that can be drawn is that, regardless of the phosphorus chemical potential, surface and interface energies always make a larger contribution to the energy variation than the elastic energy contribution. We also see that the contribution of the elastic energy is so weak that the relaxation of strain has no impact on the island morphology, which is thus mainly defined by surface/interface competition [18]. Here, we note that $R$ depends on the island shape. The energy gain provided by the transition of an equilibrium Wulff-Kaishew island ($R = 0.7$) and a similar nontruncated island ($R = 0.6$) is not sufficient to compensate the increase in the corresponding surface energy. This also applies for an island with {111} facets, where $R = 0.3$. Therefore, the gain provided by elastic relaxation is always several orders of magnitude lower than the corresponding surface/interface energy cost and therefore will not have any influence on the island shape. We finally evidence that, at a small deposited number of atoms, 2D islands may be more stable than 3D ones. A precise description of this process would, however, require taking into account edge energies, which is beyond the scope of this Rapid Communication.

The importance of elasticity can be also discussed for other III-V semiconductors. For instance, the maximization of elastic energy in AlSb assuming a biaxial stress with $R = 0.005$ leads to $\Delta F_e \approx 7.5 \times 10^2$ eV for $10^6$ atoms. This remains lower than typical surface/interface free-energy variations. In addition, a significant contribution of misfit dislocations to the interface energies is also expected for mismatched systems. In the intermediate case of GaAs, where the relaxation occurs after some monolayers, elastic energy is expected to more seriously impact the island shape before relaxation occurs [31]. In any case, after plastic relaxation, surface and interface energy competition is clearly the most important contribution to the free-energy variation, and has a prominent role in defining the shape of the initial III-V/Si islands.

From these experimental and theoretical findings, it becomes clear that the physics of III-V/Si epitaxial growth is driven by the competition between III-V surface energies, Si surface energies, and the III-V/Si interface energy. The main growth steps can be then derived and are represented in Fig. 3.

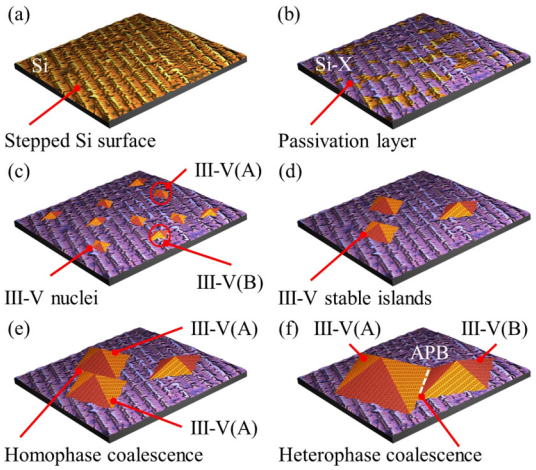


FIG. 3. Description of the proposed III-V/Si Growth steps, with (a) the 35 × 35 nm$^2$ STM image of a stepped starting Si surface. The Si surface is then covered (b) at least partially with a 2D passivation layer. Nucleation starts (c) with local epitaxial relationships and crystal polarity. Some stable islands then grow (d), independently of Si steps. If two islands of the same phase coalesce (e), they will form a larger island. If two islands having different phases coalesce (f), antiphase boundaries will appear.

Step (i): A thermal pretreatment of the Si surface possibly allows organizing Si steps [in monoatomic or biatomic layers for (001) substrates], giving rise to a monodomain or bidomain distribution at the Si surface. A 35 × 35 nm² STM image of a Si(001)-6°-off surface is provided for a realistic illustration in Fig. 3(a), but the same process occurs on Si(111).

Step (ii): The very reactive silicon surface is covered with a 2D complete or incomplete passivating layer [Fig. 3(b)]. This can be accomplished intentionally with hydrogen, for instance, in chemical vapor deposition reactors, or unintentionally with growth chamber residual atmosphere exposure, group-V initial exposure such as Si-As, Si-N, Si-Sb, or Si-P, or group-III initial exposure. This lowers the Si surface energy [see Fig. 2(b)], and promotes partial wetting conditions.

Step (iii): The nucleation starts and forms 2D or 3D small nuclei that can appear and disappear. This step is kinetically driven. The crystal polarity (we will use A and B to distinguish the two possible phases) of each nucleus is defined locally with respect to the silicon surface local orientation [Fig. 3(c)].

Step (iv): Stable 3D islands are formed and grow [Fig. 3(d)]. The epitaxial relationship and (if necessary) dislocation network (including tilt, twist) are determined locally. Each island is monophase, because the energy cost to form an antiphase boundary is too large. Consequently, once an island is stable, its polarity is preserved during its subsequent growth by an adaptation of the charge-compensated interface structure, regardless of the nature of the steps at the surface. The density of such stable islands directly defines the subsequent density/size of APDs. This density is fully determined by the kinetics of nucleation [35], mainly imposed by the migration of group-III atoms, i.e., growth temperature, nature of group-III atoms used, V/III ratio, but also the vicinality used (numbers of steps at the surface), and the nature of the passivation layer at the Si surface. The comparison between Al and Ga group-III atoms in Ref. [21] perfectly illustrates this point. Indeed, a higher density of stable islands is obtained for AlSb/Si as compared to GaSb/Si, because the Al adatom diffusion length is known to be significantly lower than the one of Ga. Kinetics also explains why APDs observed in the literature are usually larger (i.e., lower density) on nominal substrates than on vicinal ones, due to the Ehrlich-Schwoebel barrier at the step edges during the diffusion processes.

Step (v): Islands cover a large part of the Si surface, and coalescence occurs. If the two islands have the same phase, homophase coalescence leads to the formation of a larger island [Fig. 3(e)]. In this process, different tilt, twist, and dislocation network structures within individual islands may impact the structural quality of the coalesced island. If the two islands have different phases, heterophase coalescence necessarily leads, in addition to all the previous structural considerations, to the formation of an antiphase boundary [Fig. 3(b)]. The generation of APDs in III-V/Si epilayers is therefore not governed by the areal density of the monoatomic steps, as is usually suggested [3].

Overall, we finally conclude that most of the structural defects usually formed during III-V/Si epitaxy (twist, tilt, imperfect dislocation networks, or APDs) fundamentally originate from the partial wetting of III-V semiconductors on silicon, without a significant impact of elasticity. This generalized description of III-V/Si growth processes opens different routes to deeply cointegrate photonics and electronics.

The authors acknowledge Prof. P. Müller and Dr. I. Berbezier for fruitful discussions on the properties of silicon surfaces. Dr. J. Zhu is also acknowledged for giving advice on the DFT description of polar surfaces. The authors would like to thank P. Vennéguès for the AlN/Si TEM image as well as IMRA Europe S.A. for access to the JEOL 2100F microscope. This research was supported by the French National Research Agency ANTIPODE Project (Grant No. 14-CE26-0014-01), ORPHEUS Project (Grant No. ANR-17-CE24-0019-01), and Région Bretagne. The *ab initio* simulations have been performed on HPC resources of TGCC and CINES under the allocation 2017-[x20170906724] made by GENCI (Grand Equipement National de Calcul Intensif).

[1] C. Cornet, Y. Léger, and C. Robert, *Integrated Lasers on Silicon* (ISTE-Elsevier, Amsterdam, 2016).
[2] D. Derkacs, R. Jones-Albertus, F. Suarez, and O. Fidaner, J. Photonics Energy **2**, 21805 (2012).
[3] H. Kroemer, J. Cryst. Growth **81**, 193 (1987).
[4] C.-H. Choi, R. Ai, and S. A. Barnett, Phys. Rev. Lett. **67**, 2826 (1991).
[5] S. Chen, W. Li, J. Wu, Q. Jiang, M. Tang, S. Shutts, S. N. Elliott, A. Sobiesierski, A. J. Seeds, I. Ross, P. M. Smowton, and H. Liu, Nat. Photonics **10**, 307 (2016).

[6] R. Hull and A. Fischer-Colbrie, Appl. Phys. Lett. **50**, 851 (1987).
[7] F. Ernst and P. Pirouz, J. Appl. Phys. **64**, 4526 (1988).
[8] J. E. Northrup, Phys. Rev. Lett. **62**, 2487 (1989).
[9] O. Supplie, S. Brückner, O. Romanyuk, H. Döscher, C. Höhn, M. M. May, P. Kleinschmidt, F. Grosse, and T. Hannappel, Phys. Rev. B **90**, 235301 (2014).
[10] O. Romanyuk, O. Supplie, T. Susi, M. M. May, and T. Hannappel, Phys. Rev. B **94**, 155309 (2016).
[11] A. Beyer, A. Stegmüller, J. O. Oelerich, K. Jandieri, K. Werner, G. Mette, W. Stolz, S. D. Baranovskii, R. Tonner, and K. Volz, Chem. Mater. **28**, 3265 (2016).
[12] M. D. Pashley, Phys. Rev. B **40**, 10481 (1989).
[13] O. Romanyuk, T. Hannappel, and F. Grosse, Phys. Rev. B **88**, 115312 (2013).
[14] P. Kumar and C. H. Patterson, Phys. Rev. Lett. **118**, 237403 (2017).
[15] Y. P. Wang, J. Stodolna, M. Bahri, J. Kuyyalil, T. N. Thanh, S. Almosni, R. Bernard, R. Tremblay, M. D. Silva, A. Létoublon, T. Rohel, K. Tavernier, L. Largeau, G. Patriarche, A. L. Corre, A. Ponchet, C. Magen, C. Cornet, and O. Durand, Appl. Phys. Lett. **107**, 191603 (2015).
[16] P. Guillemé, M. Vallet, J. Stodolna, A. Ponchet, C. Cornet, A. Létoublon, P. Féron, O. Durand, Y. Léger, and Y. Dumeige, Opt. Express **24**, 14608 (2016).
[17] C. Robert, C. Cornet, P. Turban, T. Nguyen Thanh, M. O. Nestoklon, J. Even, J. M. Jancu, M. Perrin, H. Folliot, T. Rohel, S. Tricot, A. Balocchi, D. Lagarde, X. Marie, N. Bertru, O. Durand, and A. Le Corre, Phys. Rev. B **86**, 205316 (2012).
[18] See Supplemental Material at http://link.aps.org/supplemental/10.1103/PhysRevMaterials.2.060401 for more details on growth, microscopy, and DFT surface/interface energy calculations.
[19] Y. Takagi, H. Yonezu, K. Samonji, T. Tsuji, and N. Ohshima, J. Cryst. Growth **187**, 42 (1998).
[20] J. Tersoff and F. K. LeGoues, Phys. Rev. Lett. **72**, 3570 (1994).
[21] K. Akahane, N. Yamamoto, S. Gozu, A. Ueta, and N. Ohtani, J. Cryst. Growth **283**, 297 (2005).
[22] P. Guillemé, Y. Dumeige, J. Stodolna, M. Vallet, T. Rohel, A. Létoublon, C. Cornet, A. Ponchet, O. Durand, and Y. Léger, Semicond. Sci. Technol. **32**, 65004 (2017).
[23] J. B. Rodriguez, K. Madiomanana, L. Cerutti, A. Castellano, and E. Tournié, J. Cryst. Growth **439**, 33 (2016).
[24] A. Dupré and P. Dupré, *Théorie Mécanique de la Chaleur* (Gauthier-Villars, Paris, 1869).
[25] G.-H. Lu, M. Huang, M. Cuma, and F. Liu, Surf. Sci. **588**, 61 (2005).
[26] D. J. Chadi, Phys. Rev. Lett. **59**, 1691 (1987).
[27] P. Bogusławski, Q.-M. Zhang, Z. Zhang, and J. Bernholc, Phys. Rev. Lett. **72**, 3694 (1994).
[28] L. Geelhaar, J. Márquez, P. Kratzer, and K. Jacobi, Phys. Rev. Lett. **86**, 3815 (2001).
[29] D. K. Biegelsen, R. D. Bringans, J. E. Northrup, M. C. Schabel, and L.-E. Swartz, Phys. Rev. B **47**, 9589 (1993).
[30] J. E. Northrup, Phys. Rev. B **44**, 1419 (1991).
[31] P. Müller and R. Kern, Surf. Sci. **457**, 229 (2000).
[32] N. N. Ledentsov, *Growth Processes and Surface Phase Equilibria in Molecular Beam Epitaxy* (Springer, Berlin, 1999).
[33] A. Ponchet, D. Lacombe, L. Durand, D. Alquier, and J.-M. Cardonna, Appl. Phys. Lett. **72**, 2984 (1998).
[34] C. G. Van de Walle and J. Neugebauer, Phys. Rev. Lett. **88**, 066103 (2002).
[35] J. A. Venables, G. D. T. Spiller, and M. Hanbucken, Rep. Prog. Phys. **47**, 399 (1984).